Particle smoothers in sequential geoacoustic inversion

Caglar Yardim,[a] Peter Gerstoft, and William S. Hodgkiss
Marine Physical Laboratory, Scripps Institution of Oceanography, La Jolla, California 92093-0238

(Received 19 July 2012; revised 17 April 2013; accepted 8 May 2013)

Sequential Bayesian methods such as particle filters have been used to track a moving source in an unknown and space/time-evolving ocean environment. These methods treat both the source and the ocean parameters as non-stationary unknown random variables and track them via the multivariate posterior probability density function. Particle filters are numerical methods that can operate on nonlinear systems with non-Gaussian probability density functions. Particle smoothers are a natural extension to these filters. A smoother is appropriate in applications where data before and after the time of interest are readily available. Both past and "future" measurements are exploited in smoothers, whereas filters just use past measurements. Geoacoustic and source tracking is performed here using two smoother algorithms, the forward-backward smoother and the two-filter smoother. Smoothing is demonstrated on experimental data from both the SWellEx-96 and SW06 experiments where the parameter uncertainty is reduced relative to just filtering alone.
 [http://dx.doi.org/10.1121/1.4807819]

PACS number(s): 43.30.Pc, 43.60.Pt, 43.60.Wy, 43.60.Jn [SED] Pages: 971–981

I. INTRODUCTION

Sequential Bayesian filtering combines information on parameter variation, a function that relates acoustic measurements to unknown quantities, and a statistical model for the random perturbations in the measurements. There have been significant developments in sequential Bayesian methods, especially the particle filtering (PF) techniques, in the last decade due to both advances in theoretical signal processing and a rapid increase in computational power.[1–3]

Assume data have been collected sequentially at $t = 1{:}T$. Defining $\mathbf{y}_{1:t} = [\mathbf{y}_1, \mathbf{y}_2, \ldots, \mathbf{y}_t]$ as the set of data vectors observed at the first t steps and $\mathbf{x}_{1:t} = [\mathbf{x}_1, \mathbf{x}_2, \ldots, \mathbf{x}_t]$ as the sequence of unknown state vectors, a full inversion of this system gives the full joint posterior PDF $p(\mathbf{x}_{1:T}|\mathbf{y}_{1:T})$ of all states at all times given all the data. There are numerous Bayesian approaches that estimate the source and geoacoustic parameters. The selection is problem specific with the state dimension, data size, temporal/spatial rate of change being some of the deciding factors. Typically $\mathbf{x}$ is assumed to be changing very slowly, so one can assume $\mathbf{x}_{1:T} = \mathbf{x}$ and use $\mathbf{y}_{1:T}$ to invert for this fixed environment. In some cases, a single inversion where the entire dataset or several datasets are used can be done when the total number of state parameters is small.[4] For this case, the number of parameters can be as high as $T \times n_x$, where n_x is the number of state parameters at each time step depending on how the problem is formulated.

Assuming a more general framework where a time/range-dependent environment with a large enough state space is estimated with a dataset with large T. In such a case, it is not feasible to perform a large single inversion of all state vectors $\mathbf{x}_{1:T}$ using all of the data $\mathbf{y}_{1:T}$ to obtain $p(\mathbf{x}_{1:T}|\mathbf{y}_{1:T})$. In such cases the hard-to-obtain full joint posterior is replaced by some form of marginal PDF in time of the joint PDF. Since the data arrives sequentially, a sequential Bayesian formulation can greatly simplify the problem.

The simplest approximation is performing a series of independent inversions that only give $p(\mathbf{x}_t|\mathbf{y}_t)$ at each t. A PF provides $p(\mathbf{x}_t|\mathbf{y}_{1:t})$ and a smoother will give $p(\mathbf{x}_t|\mathbf{y}_{1:T})$, all marginals of the full posterior PDF.[1,5] More complicated and computationally intensive algorithms (such as smoothers) have posteriors closer to the full joint posterior.

A non-sequential approach estimates $\mathbf{x}_t$ without relying on information from previous or future measurements. For easy identification, the term "inversion posterior PDF" is used for the output of this case given by $p(\mathbf{x}_t|\mathbf{y}_t)$. In a sequential problem, it is inefficient computationally to perform an independent inversion at each time step. Moreover, the estimates can fluctuate significantly from step to step. Regardless, this is the approach that typically has been used in geoacoustic inversion.[6–14]

The second is a filtering approach where the "filtering posterior PDF" is given in the form $p(\mathbf{x}_t|\mathbf{y}_{1:t})$. This is the most frequently used form of sequential Bayesian estimation. Filtering enables all previous and current measurements to be used in estimating $\mathbf{x}_t$. There are numerous underwater acoustic applications such as target localization and tracking,[15–17] sequential geoacoustic inversion,[18–24] frequency tracking,[25] and spatial arrival time tracking.[26]

Finally, the third is a smoothing approach where the "smoothing posterior PDF" is given in the form $p(\mathbf{x}_t|\mathbf{y}_{1:T})$, with $T > t$. A smoother is appropriate in applications where all the data already have been observed and are readily available. Therefore, both past and "future" measurements are exploited.[27] The inclusion of future data improves estimation in comparison to a one-way filtering approach by reducing the uncertainty in the estimates. Smoothing is more computationally expensive than filtering.[28] However, recently proposed particle smoothers[5,29] have computational costs comparable to PFs. Moreover, the propagation model calculations used in geoacoustic inversion usually are more CPU intensive than

[a]Author to whom correspondence should be addressed. Electronic mail: cyardim@ucsd.edu

are the filtering/smoothing calculations. Therefore, the effects of extra smoothing calculations are secondary relative to the number of propagation model calculations.

This paper applies particle smoothing techniques to sequential geoacoustic inversion and compares the results to previous geoacoustic inversion and PF results. Two kinds of smoothers are considered here.[5,27,28] The forward-backward smoother (FBS) runs a standard PF up to T and then turns back and corrects the filter outputs at $t=T-1,\ldots,1$ while going backwards. The backward correction at t uses the information obtained from the future measurements, namely, $t=t+1,\ldots,T$. The two-filter smoother (TFS) runs two PFs moving in opposite directions, one forward filter starting at $t=1$ and one backward filter starting at $t=T$. Then the results of the two filters are merged to obtain the smoothing density. In addition to the generic TFS, a smoother that uses auxiliary sequential importance resampling (ASIR) is also adopted here.[29] The capabilities of smoothers are studied through processing range-independent (SW06) and range-dependent (SWellEx-96) experiment data.

The smoothers discussed here are given in the form of a fixed-interval smoother with $p(\mathbf{x}_t|\mathbf{y}_{1:T})$, $T>t$, since in most geoacoustic inversion applications the entire dataset is available. Even though not used in this paper, it is possible to extend this formulation to fixed-lag smoothers with $p(\mathbf{x}_t|\mathbf{y}_{1:t+\Delta T})$, for a given time lag ΔT.

II. SEQUENTIAL BAYESIAN FORMULATION

A brief summary of sequential Bayesian techniques is provided here along with the basic terminology and definitions that will be used throughout the paper. For detailed derivations refer to Refs. 1, 2, and 30.

Let $\mathbf{y}_t$ be the acoustic measurement vector at step $t=1,\ldots,T$ and $\mathbf{x}_t$ represent the state vector that include n_x parameters such as the source range, depth, and speed, array shape parameters, ocean sound speed profile (SSP), water depth, sediment thickness, sound speed, attenuation, and density. A major goal is to estimate parameters in $\mathbf{x}_t$ that evolve sequentially with time and/or space. As data $\mathbf{y}_t$ become available, the unknown parameters forming the state vector are estimated sequentially using the collective data history and prior knowledge on the variation of the state. Two equations define a state-space model,[1]

$$\mathbf{x}_t=\mathbf{f}_t(\mathbf{x}_{t-1},\mathbf{v}_t), \tag{1}$$

$$\mathbf{y}_t=\mathbf{h}_t(\mathbf{x}_t,\mathbf{w}_t). \tag{2}$$

The *state equation* Eq. (1), describes the transition of $\mathbf{x}_t$ with t and assumes that states follow a first order Markov process.[1,31] Function $\mathbf{f}_t$ is known and relates the state vector at step t to that at step $t-1$. Variable $\mathbf{v}_t$ is the process or state noise with a PDF $p(\mathbf{v}_t)$.

The *measurement equation* (or observation equation), Eq. (2), relates measurements $\mathbf{y}_t$ to state vector $\mathbf{x}_t$ through a known function $\mathbf{h}_t$. Variable $\mathbf{w}_t$ is the measurement noise with a PDF $p(\mathbf{w}_t)$.

The state and measurement noise terms $\mathbf{v}_t$ and $\mathbf{w}_t$ can be additive or multiplicative and are incorporated into the state and measurement through nonlinear functions $\mathbf{f}_t$ and $\mathbf{h}_t$, respectively. The formulation includes fully dynamic, non-stationary cases, where in addition to the state vector $\mathbf{x}_t$ and data $\mathbf{y}_t$, functions $\mathbf{f}_t$ and $\mathbf{h}_t$, and noise components $\mathbf{v}_t$ and $\mathbf{w}_t$ all can change with t.

The objective of a sequential Bayesian method is to track the variability of the multidimensional (n_x-D) posterior PDF of $\mathbf{x}_t$. This enables any desired statistical quantity (such as mean, covariance, mode, maximum *a posteriori* estimate, credible intervals, marginal posterior PDFs of any desired parameter) to be computed at will.

Using Bayes theorem gives

$$p(\mathbf{x}_t|\mathbf{y}_{1:t})\propto p(\mathbf{y}_t|\mathbf{x}_t)p(\mathbf{x}_t|\mathbf{y}_{1:t-1}), \tag{3}$$

where the likelihood $\mathcal{L}(\mathbf{x}_t)=p(\mathbf{y}_t|\mathbf{x}_t)$ obtained from the new data $\mathbf{y}_t$ is combined with the prior knowledge $p(\mathbf{x}_t|\mathbf{y}_{1:t-1})$ to estimate $\mathbf{x}_t$. It is possible to compute $p(\mathbf{x}_t|\mathbf{y}_{1:t-1})$ as a function of $\mathbf{x}_{t-1}$ by starting from the joint PDF $p(\mathbf{x}_t,\mathbf{x}_{t-1}|\mathbf{y}_{1:t-1})$ and integrating out $\mathbf{x}_{t-1}$,

$$\begin{aligned}p(\mathbf{x}_t|\mathbf{y}_{1:t-1})&=\int p(\mathbf{x}_t,\mathbf{x}_{t-1}|\mathbf{y}_{1:t-1})\mathrm{d}\mathbf{x}_{t-1}\\&=\int p(\mathbf{x}_t|\mathbf{x}_{t-1},\mathbf{y}_{1:t-1})p(\mathbf{x}_{t-1}|\mathbf{y}_{1:t-1})\mathrm{d}\mathbf{x}_{t-1}.\end{aligned} \tag{4}$$

Note that $p(\mathbf{x}_t|\mathbf{x}_{t-1},\mathbf{y}_{1:t-1})=p(\mathbf{x}_t|\mathbf{x}_{t-1})$ since, given $\mathbf{x}_{t-1}$, *any data from* 1: $t-1$ become irrelevant due to the first order Markovian nature of the state vector as expressed in Eq. (1). The filtering posterior PDF $p(\mathbf{x}_t|\mathbf{y}_{1:t})$ is then expressed as a function of the posterior at the previous step $p(\mathbf{x}_{t-1}|\mathbf{y}_{1:t-1})$ by inserting the integral form of $p(\mathbf{x}_t|\mathbf{y}_{1:t-1})$ back into Eq. (3),

$$p(\mathbf{x}_t|\mathbf{y}_{1:t})\propto p(\mathbf{y}_t|\mathbf{x}_t)\int p(\mathbf{x}_t|\mathbf{x}_{t-1})p(\mathbf{x}_{t-1}|\mathbf{y}_{1:t-1})\mathrm{d}\mathbf{x}_{t-1}. \tag{5}$$

Sequential Bayesian methods utilize this formulation whereby the evolving filtering posterior PDF can be computed recursively as new data $\mathbf{y}_t$ become available.

For strongly nonlinear/non-Gaussian problems, a particle filter (PF) is appropriate.[1] The non-Gaussian filtering posterior PDFs are approximated by creating a set of $i=1,\ldots,N_p$ particles $\mathbf{x}_t^i$, each with weight w_t^i, where

$$\begin{aligned}&\chi_t:\{\mathbf{x}_t^i,w_t^i\}_{i=1}^{N_p}\\&p(\mathbf{x}_t|\mathbf{y}_{1:t})\cong\sum_{i=1}^{N_p}w_t^i\delta(\mathbf{x}_t-\mathbf{x}_t^i).\end{aligned} \tag{6}$$

Hence, the purpose of a PF is to track in time t these particles and their weights as they pass through nonlinear equations Eqs. (1)–(2). The filtering posterior PDF can be constructed at any time from the current values and weights of the particles using Eq. (6). This enables the computing of any desired quantity such as the minimum mean square error estimate, variance, and marginal distributions by taking integrals of the posterior PDF,

$$I = \int g(\mathbf{x}_t) p(\mathbf{x}_t|\mathbf{y}_{1:t}) \mathrm{d}\mathbf{x}_t, \tag{7}$$

where $g(\mathbf{x}_t) = \mathbf{x}_t$ for the mean, $g(\mathbf{x}_t) = (\mathbf{x}_t - \mu_{\mathbf{x}})^2$ for the variance, and $g(\mathbf{x}_t) = \delta[\mathbf{x}_t - \mathbf{x}_t(i)]$ for the ith element marginal distribution.

Two types of PFs are used in this work. Sequential importance resampling[32] (SIR) is the most commonly used type of PF. In addition, the auxiliary SIR[33] (ASIR) is also used since the two-ASIR smoother requires the PF to be of the ASIR type. For detailed descriptions of SIR and ASIR see Ref. 1. Since the ASIR PF has not been used in geoacoustic tracking before, the ASIR PF algorithm is summarized in Table III of the Appendix for completeness.

Consistent with our previous work,[34] SIR type filters are used as the base PFs. These filters are more sensitive to outliers and impoverishment issues. It is possible to implement PFs such as a regularized PF[1] or a Markov chain Monte Carlo (MCMC) PF similar to the one in Ref. 21 that can handle better the problem of outliers and the impoverishment issue. Except for the two-ASIR smoother,[29] generic FBS and TFS implementations[5,28] can be implemented with any type of PF.

III. SMOOTHING

An overview of the smoothers used in this paper is provided here. The basic philosophy and differences between existing smoothing algorithms[5,27–29] are summarized along with how they can be implemented in a geoacoustic inversion setting.

In geoacoustics, the measurements usually involve a source or receiver moving along a pre-determined path for a fixed time-interval. Often, the whole observation data set $\mathbf{y}_{1:T}$ or at least some future data $\mathbf{y}_{1:t+\Delta T}$ is available for analysis. To use the entire dataset, a fixed-interval smoother is adopted here.

In this approach, time is made to go both forward and backward while maintaining the physical relationships between measurements and model parameters. The ability to use "future" data $\mathbf{y}_{t+1:T}$ in addition to $\mathbf{y}_{1:t}$ improves the estimates and their uncertainties relative to a PF. The smoothing posterior PDF $p(\mathbf{x}_t|\mathbf{y}_{1:T})$ for $t = 1,\ldots, T$ is the marginal in time of the joint posterior PDF $p(\mathbf{x}_{1:T}|\mathbf{y}_{1:T})$ and techniques that obtain $p(\mathbf{x}_t|\mathbf{y}_{1:T})$ are termed smoothing algorithms.[5,28]

Kalman smoothers can be used under linear/Gaussian assumptions for the state and measurement equations, Eqs. (1)–(2). For nonlinear/non-Gaussian systems, such as most geoacoustic inversion cases, numerical particle smoothers can be used. These are implemented with the same basic philosophy as the PF where the smoothing density is represented by N_p smoothing particles $\mathbf{x}^i_{t|T}$ and their weights $w^i_{t|T}$ as a weighted sum,

$$\chi^S_t = \{\mathbf{x}^i_{t|T}, w^i_{t|T}\}_{i=1}^{N_p}, \tag{8}$$

$$p(\mathbf{x}_t|\mathbf{y}_{1:T}) = \sum_{i=1}^{N_p} w^i_{t|T} \delta(\mathbf{x}_t - \mathbf{x}^i_{t|T}). \tag{9}$$

It is possible to divide smoothers into two broad categories: forward-backward (FBS) and two-filter (TFS) smoothers.[5,28]

A. Forward-backward smoother

The geoacoustic FBS is based on a classical forward-running PF for $t = 1,\ldots, T$ that gives the set $\{\mathbf{x}^i_t, w^i_t\}_{i=1}^{N_p}$ representing the filtering density $p(\mathbf{x}_t|\mathbf{y}_{1:t})$. Hence, it readily can be implemented on the existing geoacoustic PF results.[20,22,34] The algorithm runs a backward correction which updates the weights of the forward PF particles $w^i_t \rightarrow w^i_{t|T}$ so that they represent the smoothing PDF $p(\mathbf{x}_t|\mathbf{y}_{1:T})$. No new smoothing particles are created.[35]

The integral that needs to be solved sequentially in a FBS is given by expressing the smoothing density in terms of the filtering density. Similar to Eq. (4) it is possible to express $p(\mathbf{x}_t|\mathbf{y}_{1:T})$ as a function of $\mathbf{x}_{t+1}$ by starting from the joint PDF $p(\mathbf{x}_t, \mathbf{x}_{t+1}|\mathbf{y}_{1:T})$ and integrating out $\mathbf{x}_{t+1}$,

$$p(\mathbf{x}_t|\mathbf{y}_{1:T}) = \int p(\mathbf{x}_t|\mathbf{x}_{t+1}, \mathbf{y}_{1:t}) p(\mathbf{x}_{t+1}|\mathbf{y}_{1:T}) \mathrm{d}\mathbf{x}_{t+1}. \tag{10}$$

The smoothing density then can be obtained by computing the integral in Eq. (10). This results in[35]

$$p(\mathbf{x}_t|\mathbf{y}_{1:T}) \cong \sum_{i=1}^{N_p} w^i_{t|T} \delta(\mathbf{x}_t - \mathbf{x}^i_t), \tag{11}$$

$$w^i_{t|T} = \sum_{j=1}^{N_p} \frac{w^i_t p(\mathbf{x}^j_{t+1}|\mathbf{x}^i_t)}{\sum_{k=1}^{N_p} w^k_t p(\mathbf{x}^j_{t+1}|\mathbf{x}^k_t)} w^j_{t+1|T}, \tag{12}$$

where $w^i_{T|T} = w^i_T$. This is a backward recursion starting from $t = T$ and going back in time, estimating the integral by correcting the filter weights using the "future" information. Hence, to compute the smoothing density, all we need to do is to replace the filtering weight w^i_t with the new smoothing weight $w^i_{t|T}$ given by Eq. (12) for each particle x^i_t. This basic mechanism of the FBS is shown in Fig. 1(a). Since the FBS uses the same particles as the forward PF, i.e., $\mathbf{x}^i_{t|T} = \mathbf{x}^i_t$, only the weights are updated. Hence, if the initial forward PF particle cloud $\{\mathbf{x}^i_t\}_{i=1}^{N_p}$ poorly corresponds to the smoothing PDF, the FBS will suffer.

B. Two-filter smoother

Another way of writing the smoothing density is to use Bayes' rule instead of the integral formulation of the FBS,

$$p(\mathbf{x}_t|\mathbf{y}_{1:T}) = p(\mathbf{x}_t|\mathbf{y}_{1:t-1}, \mathbf{y}_{t:T}) \tag{13}$$

$$= \frac{p(\mathbf{x}_t|\mathbf{y}_{1:t-1}) p(\mathbf{y}_{t:T}|\mathbf{x}_t)}{p(\mathbf{y}_{t:T}|\mathbf{y}_{1:t-1})} \tag{14}$$

$$\propto \underbrace{p(\mathbf{x}_t|\mathbf{y}_{1:t-1})}_{\text{forward PF}} \times \underbrace{p(\mathbf{y}_{t:T}|\mathbf{x}_t)}_{\text{backward inf. filter}}. \tag{15}$$

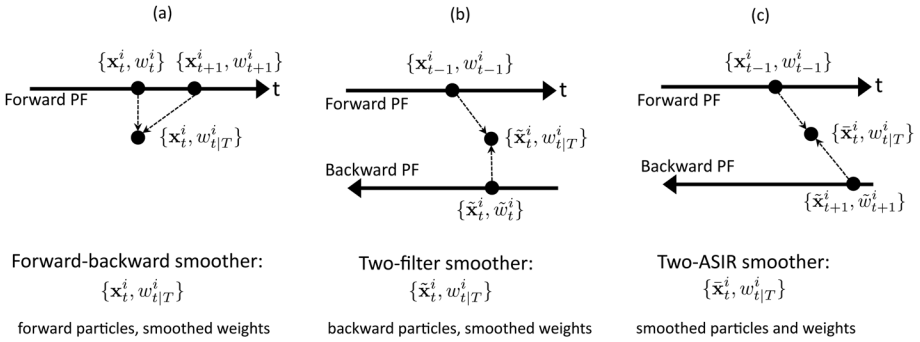

FIG. 1. Diagram that shows how smoothing weights and particles are selected for: (a) Generic FBS, (b) generic TFS, and (c) two-ASIR smoother.

The first part of the equation is given by a forward PF. The second term is called the backward information filter[5] which can be replaced by an equivalent backward PF denoted by $\tilde{p}(\cdot)$. This is done using Bayes' rule, $p(\mathbf{y}_{t:T}|\mathbf{x}_t) \propto \tilde{p}(\mathbf{x}_t|\mathbf{y}_{t:T})/\tilde{p}(\mathbf{x}_t)$.

Following Ref. 5, the smoothing PDF can be computed by running a backward PF in addition to the forward PF and using both to compute Eq. (15),

$$p(\mathbf{x}_t|\mathbf{y}_{1:T}) \cong \sum_{i=1}^{N_p} w_{t|T}^i \delta(\mathbf{x}_t - \tilde{\mathbf{x}}_t^i), \tag{16}$$

$$w_{t|T}^i = \frac{\tilde{w}_t^i}{\tilde{p}(\tilde{\mathbf{x}}_t^i)} \sum_{j=1}^{N_p} w_{t-1}^j p(\tilde{\mathbf{x}}_t^j|\mathbf{x}_{t-1}^j). \tag{17}$$

The TFS uses the particles obtained by the backward PF, i.e., $\mathbf{x}_{t|T}^i = \tilde{\mathbf{x}}_t^i$ and only the weights are recalculated.[5] This basic mechanism of the TFS is shown in Fig. 1(b). Thus, if the backward PF cloud $\{\tilde{\mathbf{x}}_t^i\}_{i=1}^{N_p}$ poorly corresponds to the smoothing PDF, the TFS will suffer.

This problem has been addressed in a recently proposed TFS that uses the ASIR PF as both the forward and backward PFs.[29] This two-ASIR smoother given in Fig. 1(c) not only computes new smoothing weights $w_{t|T}^i$ but also draws new smoothing particles $\mathbf{x}_{t|T}^i$. The two-ASIR smoother has been shown to reduce the parameter uncertainty relative to other smoothing algorithms in a non-volcanic tremor source tracking problem.[36] The two-ASIR algorithm is summarized in Table IV of the Appendix.

C. Practical considerations for a geoacoustic smoother

The primary concern with implementing a geoacoustic smoother is the computational cost. In a geoacoustic inversion context there are two sources of added complexity.

The first is the number of additional smoothing calculations required. Classical FBS or TFS algorithms require a large number of smoothing calculations, typically on the order of N_p^2, $O(N_p^2)$. Therefore, the demand on CPU time for inversions will grow rapidly with increasing N_p. However, there have been significant improvements in particle smoothing in the last decade both in terms of efficiency and accuracy. Recently proposed FBS and TFS algorithms such as those discussed in Refs. 28 and 29 can operate with an order of complexity of $O(N_p)$ under the right conditions.

The second and the more important factor in a sequential geoacoustic inversion setting is the effect of smoothing on the number of forward model runs. In geoacoustic tracking, each forward PF particle is generated using a propagation model such as a parabolic equation or a normal mode model. Hence, the most CPU intensive part of the process is the propagation model computation for each particle. Anytime a new particle is created the forward model is run to compute its likelihood. In FBS, the backward correction uses the same particles as the forward PF so there are no additional propagation model calculations. The classical TFS has twice the forward model computational cost of the FBS since it is composed of two PFs. Unlike classical smoothers, the two-ASIR smoother samples its own smoothing particles. Hence the forward, backward, and smoothing particles created for the two-ASIR smoother requires three times the number of propagation model runs of the FBS. For strongly range-dependent geoacoustic inversions that use propagation models with intense CPU calculations, this can be a disadvantage.

In geoacoustic smoothing, the total computational cost is a combination of the two factors discussed above with the smoothing computations usually less demanding than the propagation model calculations. Different smoothers will be faster depending on the propagation model chosen.

IV. STATE EQUATION AND THE LIKELIHOOD FORMULATION

The state equation is formed from two blocks—a source and an environmental parameter block. In the source block, three source parameters (i.e., source depth, range, and radial speed) are grouped as $\mathbf{s}_t = [z_s \quad r_s \quad v_s]_t'$. Using a constant velocity (CV) track model for the source, the state model for the source block becomes

$$\begin{bmatrix} z_s \\ r_s \\ v_s \end{bmatrix}_t = \begin{bmatrix} 1 & 0 & 0 \\ 0 & 1 & \Delta t \\ 0 & 0 & 1 \end{bmatrix} \begin{bmatrix} z_s \\ r_s \\ v_s \end{bmatrix}_{t-1} + \begin{bmatrix} 1 & 0 \\ 0 & \frac{\Delta t^2}{2} \\ 0 & \Delta t \end{bmatrix} \begin{bmatrix} v_z^s \\ v_a^s \end{bmatrix}_t, \tag{18}$$

where v_z^s and v_a^s are random variables representing the variation in source depth and acceleration, respectively.[1] This results in a vector-matrix form,

$$\mathbf{s}_t = \mathbf{F}^s \mathbf{s}_{t-1} + \mathbf{B}^s \mathbf{v}_t^s. \tag{19}$$

Assuming that the environmental parameters $\mathbf{m}_t$ change much slower than Δt, the time between successive measurements, the full state equation for the state vector $\mathbf{x}_t = [\mathbf{s}_t' \quad \mathbf{m}_t']'$ is given by

$$\begin{bmatrix} \mathbf{s} \\ \mathbf{m} \end{bmatrix}_t = \begin{bmatrix} \mathbf{F}^s & 0 \\ 0 & \mathbf{I} \end{bmatrix} \begin{bmatrix} \mathbf{s} \\ \mathbf{m} \end{bmatrix}_{t-1} + \begin{bmatrix} \mathbf{B}^s & 0 \\ 0 & \mathbf{I} \end{bmatrix} \begin{bmatrix} \mathbf{v}^s \\ \mathbf{v}^m \end{bmatrix}_t. \tag{20}$$

The PF and smoothers used for both SW06[22] and SWellEx-96[20] data sets have the same state space form given here, just some of the individual parameters are different.

The analyses of both data sets also use the same likelihood formulation based on the Bartlett objective function that is coherent across the array and incoherent across frequency. Assume $\mathbf{d}(\mathbf{x}_t, f_j)$ is the acoustic field vector one would predict for the state $\mathbf{x}_t$ at each frequency f_j, calculated using an acoustic propagation model. Defining the cross spectral density matrix for the jth frequency $\mathbf{C}_j = \mathrm{E}[\mathbf{y}_k(f_j)\, \mathbf{y}_k(f_j)^{\mathrm{H}}]$, the likelihood expression is written as

$$\mathcal{L}(\mathbf{x}_t) = \prod_{j=1}^{n_f} \left[\frac{n_h}{\mathrm{e}\pi \phi_j(\mathbf{x}_t)} \right]^{n_h}. \tag{21}$$

$$\phi_j(\mathbf{x}_t) = \mathrm{tr}\ \mathbf{C}_j - \frac{\mathbf{d}(\mathbf{x}_t, f_j)^{\mathrm{H}} \mathbf{C}_j \mathbf{d}(\mathbf{x}_t, f_j)}{\mathbf{d}(\mathbf{x}_t, f_j)^{\mathrm{H}} \mathbf{d}(\mathbf{x}_t, f_j)}, \tag{22}$$

where tr is the trace operation, n_f and n_h are the number of frequencies and array elements, respectively, and ϕ_j represents the Bartlett objective function. For a detailed derivation see Ref. 20.

The quasi-range-independent SW06 data is analyzed using an ASIR framework. Filtering/smoothing posterior PDFs and computational costs of an ASIR type PF, FBS, and TFS (as a two-ASIR TFS) in a geoacoustic inversion setting are calculated and a performance comparison is made in terms of RMS error reduction.

Filtering also is compared to smoothing with the range-dependent SWellEx-96 data, this time in a SIR framework. The ASIR framework is not used here since the filters assume a range-independent geoacoustic parameter variability model in their state equations, Eq. (20), while in fact there is a strong range dependence (water depth dropping from 260 m to 90 m after 30 filter time steps). For the PF to perform well in this case, the process noise needs to be increased to compensate for the model variation mismatch. A drawback of ASIR is that it performs worse than SIR in the presence of large process noise.[1] If an ASIR type filter and smoother is to be run in this case, one way of reducing the process noise would be to reduce the time between time steps from their current 1 min and hence increase the number of time steps. Alternatively, the rate of change of the environmental parameters can be included as new parameters in the state equation. Here, we use a SIR type PF and FBS instead to demonstrate a reduction in uncertainty of the parameter estimates in the SWellEx-96 data.

Since smoothers use more information relative to filters, they tend to reduce the uncertainty in the parameter estimates. As always with Bayesian geoacoustic inversion methods, the calculated uncertainty in the parameter estimates is a direct function of the accuracy of the state and observation models given in Eqs. (1)–(2). Unaccounted-for errors (e.g., simplified geoacoustic models, propagation model errors, etc.) will affect the quality of the inversion results including the uncertainties.

The performance metrics for comparing the filter and smoothers are

$$\mathrm{RTAMS}(i) = \left\{ \sum_{t=t_1}^{t_2} \sum_{j=1}^{N_p} \frac{[\mathbf{x}_t^j(i) - \hat{\mathbf{x}}_t(i)]^2}{(t_2 - t_1 + 1) N_p} \right\}^{1/2}, \tag{23}$$

$$\mathrm{Improv.} = \frac{\mathrm{RTAMS_{PF}} - \mathrm{RTAMS_{smoother}}}{\mathrm{RTAMS_{PF}}}, \tag{24}$$

where $\mathbf{x}_t^j(i)$ is the ith parameter at time index t for the jth particle, $\hat{\mathbf{x}}_t(i)$ is either the true value or the estimator mean of the parameter depending on whether a direct measurement is available or not. RTAMS is the root time averaged mean square error[1] calculated for the interval $[t_1, t_2]$, and Eq. (24) is used to calculate the performance improvement of a smoother with respect to the PF.

V. DEMONSTRATION OF SMOOTHING WITH SW06 DATA

Both FBS and TFS are tested on data collected in a relatively constant water depth, from an area northwest of the shelfbreak during the SW06 Experiment. The smoothers are compared not only to each other but also to a PF solution.

A. SW06 experiment

In the selected track, the geoacoustic parameters do not vary much. The largest variation in the environmental parameters comes from the water column SSP which is known to fluctuate significantly with time. Data were collected on 28 August 2006 (JD240), 00:50–01:20 UTC. The source location, bathymetry, array parameters, and the seabed properties are assumed unknown. The R/V Knorr approached the fixed vertical array at a speed of 5 knots while towing a source at 25–30 m depth and emitting a multitone comb at frequencies 303, 403, 503, 703, 953 Hz. The last 10 min section of the track ranging from 3.7 to 1.7 km is used. The data from this track also were analyzed in Refs. 37 and 38.

The received time-series was split into snapshots with 50% overlap and converted to the frequency domain using a 2^{18}-point FFT. The data cross-spectral density matrices (CSDMs) were computed as the outer products of 7 snapshots representing a time epoch of 20 s spread across 50 m in range, hence 30 time steps for a track length of 10 min.

The environment model given in Fig. 2 is used for each range. For this case, the sediment sound speed is taken as a

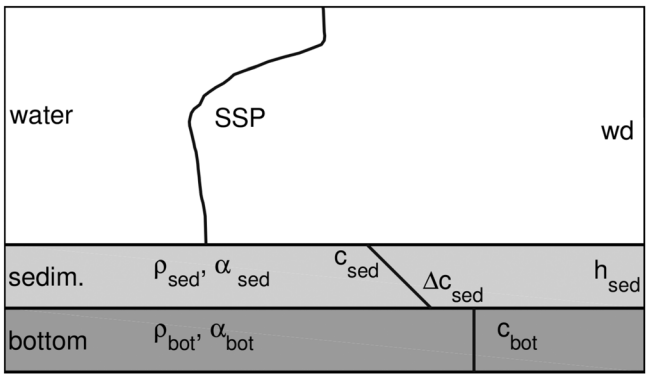

FIG. 2. Geoacoustic model used for both SW06 and SWellEx-96 environments in the PF, FBS, and TFS.

constant with $\Delta c_{sed} = 0$. An empirical orthogonal function (EOF) analysis of the SSP was carried out using 16 CTD measurements along the 80 m isobath track from JD239 19:17 to JD243 20:16 UTC giving a mean profile together with the first 3 EOFs (accounting for 90% of the variance in ocean SSP).[37] The SSP is tracked by tracking the EOF coefficients. Since the track mostly is flat and range-independent, the normal mode code SNAP[39] is used. Hence, the range-independent effective seabed model and SSP are tracked together with the moving ship parameters. The state consists of 12 parameters including source depth, range, and speed, VLA tilt, first array depth, water depth, sediment thickness, sediment top and bottom layer sound speeds, and the EOF coefficients for the water column SSP. Density and attenuation are held fixed.

B. Filtering and smoothing results

Here the same settings, prior PDFs, state, and measurement noise statistics as the ones reported in Ref. 22 are used to initialize the filters and smoothers. First an ASIR PF is used to track the source and the environment. This is followed by a FBS that used the previous ASIR result and performed a backward correction to obtain the smoothing posterior PDF. Finally, a TFS in the form of a two-ASIR smoother is implemented, where in addition to the forward ASIR PF, a backward ASIR PF is run and the results of these two PFs are merged according to the algorithm given in the Appendix.

RTAMS is calculated starting from $t_1 = 2$ min so that the initial variation will not affect the performance calculations. The PF, FBS, and the two-ASIR smoother results are shown in Figs. 3–5, respectively, along with a comparison of their performance metrics in Table I.

Along the 10 min trajectory, the source depth oscillates between 27 and 31 m while the source gets closer from 3.7 to 1.7 km. All three algorithms were able to track the source parameters successfully. Other source parameters such as the source range are also tracked well.

Water depth fluctuates between 81 and 78 m along the path[38] with the water depth at 81 m at the start of the track and gets slightly shallower on average as the ship moves towards the VLA. The effective range-independent water depth PDF also supports this. Both smoothers give almost

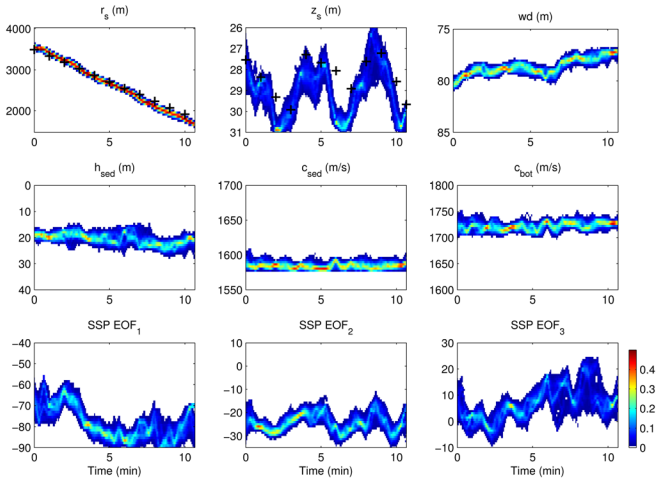

FIG. 3. (Color online) SW06 ASIR-type PF results: Variation of 1-D marginal filtering posterior PDFs for source and sediment parameters, and the EOF coefficients for water column SSP. (+) represents GPS range and depth sensor measurements.

identical RTAMS and improvement percentages of a little over 50%.

The changing water column SSP is obtained through tracking the three EOF coefficients. The fluctuations in the EOF coefficients and their effects on the SSP itself is analyzed in the next section.

The sediment sound speed stays between 1580 and 1605 m/s, sediment thickness 17–22 m, and the bottom sound speed 1690–1750 m/s, respectively, along the track. Even though detailed range-dependent ground truth measurements do not exist, the results compare favorably with previous studies that inverted data from the same area with an average c_{sed} of 1599 m/s in Ref. 38 (1604 m/s in Ref. 37), h_{sed} of 21.1 (24) m, and c_{bot} of 1740 (1739) m/s. Sediment thickness is consistent with other studies where the R-reflector is found to be around 20 m below the seafloor.[40–43] Previous studies[13,14,44] also reported similar sediment sound speed results.

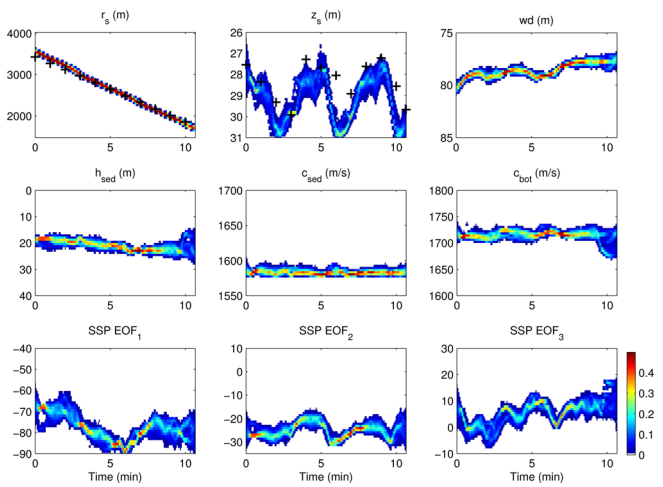

FIG. 4. (Color online) SW06 ASIR-type FBS results: Variation of 1-D marginal smoothing posterior PDFs for source and sediment parameters, and the EOF coefficients for water column SSP. (+) represents GPS range and depth sensor measurements.

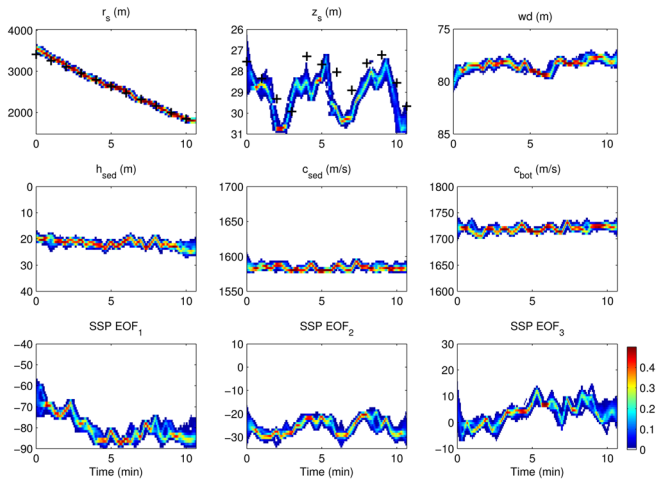

FIG. 5. (Color online) SW06 TFS results (two-ASIR smoother): Variation of 1-D marginal smoothing posterior PDFs for source and sediment parameters, and the EOF coefficients for water column SSP. (+) represents GPS range and depth sensor measurements.

The two-ASIR smoother has significant improvement over the FBS in estimating sediment and bottom sound speed. The improvements in the sediment thickness and the EOF coefficients are less pronounced. As expected, the PDFs of the PF given in Fig. 3 show a larger uncertainty compared to smoothing PDFs in Figs. 4 and 5 due to the fact that the PF uses less information to estimate the parameters sequentially. Both smoothers do well in terms of error variance reduction with the FBS and TFS giving an average of 47% and 62% improvement over the PF, respectively.

Filter convergence is an important and complex issue. It is important to use a PF with sufficient particles that converged to its filtering density $p(\mathbf{x}_t|\mathbf{y}_{1:t})$ before running a smoother on it. For the SIR type PFs, the resampling stage creates multiple copies of high likelihood particles. This results in a N_p value tightly related to the number of state variables.[45] Moreover, the importance density in SIR also affects convergence. A good sampling density[46] results in N_p increasing linearly with n_x but N_p increases exponentially with n_x when the importance density is poorly chosen. A practical approach is used here to determine N_p. A preliminary set of PFs with increasing number of N_p's are run and the outputs are compared. N_p is then obtained when the change in the PF results drop below a threshold. A detailed convergence discussion on sequential Monte Carlo methods can be found in Ref. 47.

C. Sound speed profile estimation

The marginal filtering/smoothing posterior PDFs for the water column SSP are obtained from the marginal posterior of the three EOF coefficients. The SSP measurement at the track location is not available but three close measurements at locations SW30, SW31, and Shark (Fig. 2 in Ref. 22) at the time of the experiment confirm the rapid SSP variation in the region. The maximum *a posteriori* (MAP) PF SSP estimates at four different times along the track given in Fig. 6(a) (relative to the time-averaged MAP PF SSP solution) fit within the variation measured at the discrete depths of the sensors. The marginal SSP posteriors are compared in Figs. 6(b)–6(e). In most cases, the result is a sharper smoothing posterior PDF with the two-ASIR smoother performing better then the FBS. The largest improvements are at the depths of 15–20 m and 30–35 m.

The standard deviation (STD) of the water column sound speed as a function of depth and time are given in Fig. 7 to quantify the uncertainty in estimates obtained via filtering/smoothing. All three algorithms show larger STD between 7 and 9 min where the value can be in excess of 3.5 m/s for the PF. The average STD between 15 and 40 m deep for $t = 1 - 10$ min is 1.2, 0.8, and 0.5 m/s for the PF, FBS, and the two-ASIR smoother, respectively.

D. Projection of environmental uncertainty into transmission loss

Finally, the filtering/smoothing environmental posterior PDFs are used to predict a parameter-of-interest such as the transmission loss (TL) over a given range in Fig. 8. This is done by integrating over the source parameters of the multi-dimensional posterior PDF and then using this marginal PDF that statistically characterizes the environment in TL calculations. The TL is then computed for all the particles (each representing a possible environment) to construct the TL PDF. Figure 8 is obtained using $z_s = 30$ m, $z_r = 35$ m, $f = 300$ Hz using the environmental posterior PDF at $t = 8$ min.

Again the smoothers outperform the PF. Note that the TL obtained from the filtering posterior PDF is usually multi-peaked and typically has a spread of 5–10 dB for the peak and 20–25 dB for the trough, similar to the values obtained in Refs. 48 and 49. In contrast, the smoothing algorithms seem to have a sharper peak in most cases [Figs. 8(d) and 8(e)]. Thus, inclusion of future data helps the smoother eliminate one or more of the peaks seen in the filtering posterior PDFs.

TABLE I. SW06 Filter-smoother comparison.

Parameter	r_s (m)	z_s (m)	wd (m)	h_{sed} (m)	c_{sed} (m/s)	c_{bot} (m/s)	SSP EOF_1	EOF_2	EOF_3	Avg.
$RTAMS_{PF}$	23.5	0.5	0.4	2.4	4.6	7.3	3.4	2.6	4.1	-
$RTAMS_{FBS}$	8.9	0.4	0.2	0.8	2.9	4.8	2.1	1.3	1.6	-
$RTAMS_{Two\text{-}ASIR}$	12.1	0.2	0.2	0.5	1.9	2.2	1.5	1.2	1.1	-
FBS % improv.	62	20	55	66	36	34	37	49	61	47
Two-ASIR % improv.	48	58	54	78	65	70	57	54	74	62

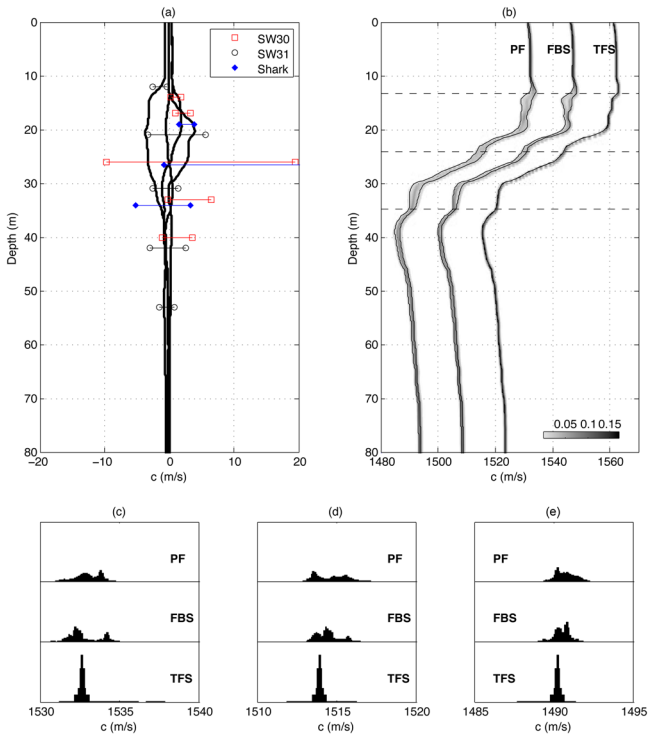

FIG. 6. (Color online) SW06 SSP results: (a) Variation of SSP relative to the time-averaged MAP PF SSP. MAP water column SSPs at $t = 2.5$, 5, 7.5, and 10 min plotted together. Horizontal lines represent the range of sound speed values measured within 20 min of the track at various depths and locations. (b) Filtering/smoothing posterior PDFs of the SSP at $t = 5$ min plotted together. FBS and TFS results are shifted for easy comparison. Solid lines represent the 95% credibility intervals. Horizontal marginal cuts at depths (c) 13 m, (d) 24 m, and (e) 35 m for all three methods.

Both smoothers try to obtain the same smoothing PDF, but there are sometimes differences between the smoothers with the same number of particles. Note that the TFS smoothing particles are selected specifically to represent

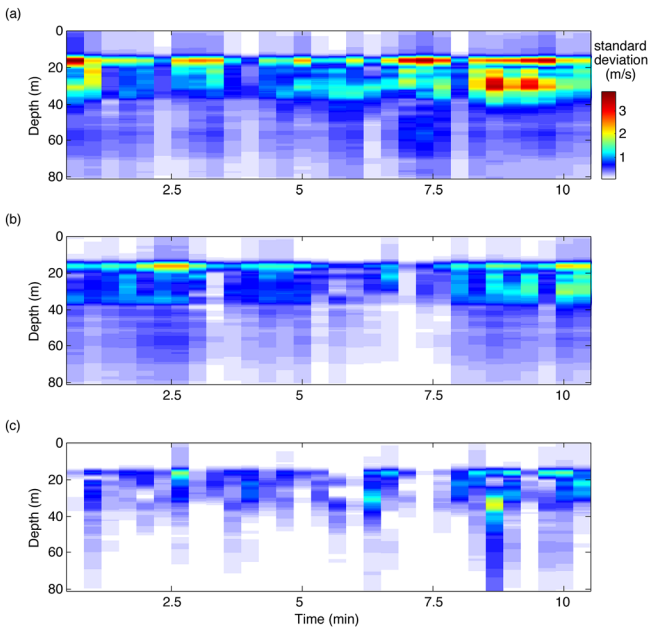

FIG. 7. (Color online) SW06 SSP results: Standard deviation (in m/s) for the sound speed estimates at all depths along the track for (a) PF, (b) FBS, and (c) TFS.

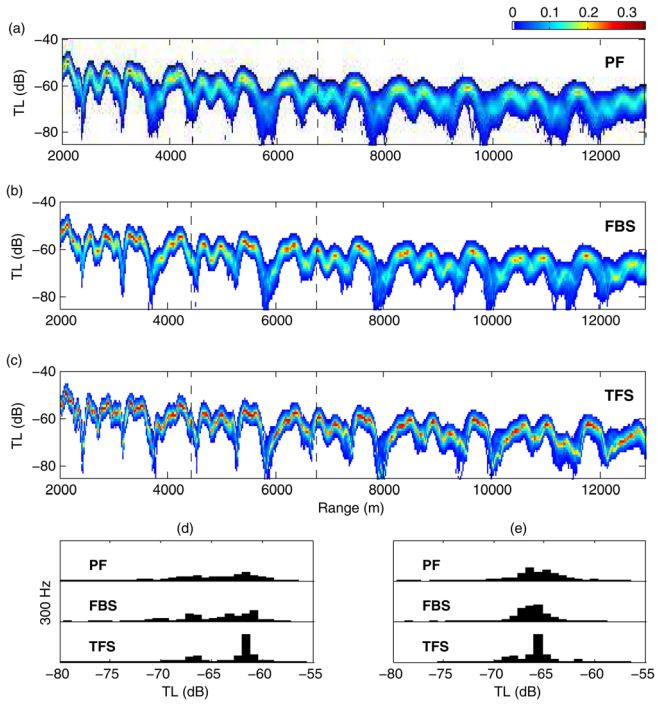

FIG. 8. (Color online) SW06 transmission loss (TL) predictions at $z_s = 30$ m, $z_r = 35$ m, $f = 300$ Hz and $t = 8$ min: The posterior PDF of TL vs range for (a) PF, (b) FBS, and (c) TFS. Horizontal marginal cut at ranges of (c) 4500 m (trough) and (d) 6700 m (peak) for all three methods.

the smoothing PDF whereas FBS uses filtering particles. This creates the same problem encountered in classical importance sampling (IS): the larger the difference between the sampling IS density from the true underlying PDF, the larger the error in the IS estimate is going to be.[50] Smoothing and filtering particle sets can also differ in situations where the observations after time t provide significant information about the state $\mathbf{x}_t$. In these cases, the TFS can "substantially outperform" the FBS.[51]

VI. DEMONSTRATION OF SMOOTHING WITH SWellEx-96 data

Filtering also is compared to smoothing using the acoustic data collected during the Shallow Water evaluation cell Experiment (SWellEx-96).[52] First a SIR type PF is run similar to the one reported in Ref. 20, and then a FBS backward correction is done on the SIR PF particles.

A. SWellEx-96 experiment

The experiment was conducted in May 1996 off the coast of San Diego, CA, near Point Loma. A 118 m VLA was deployed from R/P FLIP in 216.5 m deep water north of Loma Canyon. Event S9 is selected here since the track is perpendicular to bathymetric lines giving the highest rate of change of environment as ship moves into shallower water.[53] The source was towed at 2.6 m/s at a depth of 55 m. The transmission was a comb signal composed of 13 frequencies from 49 to 388 Hz. The water column sound speed profile was obtained by conductivity-temperature-depth (CTD) measurements. Cross-spectral density matrices (CSDMs) are estimated for each frequency at

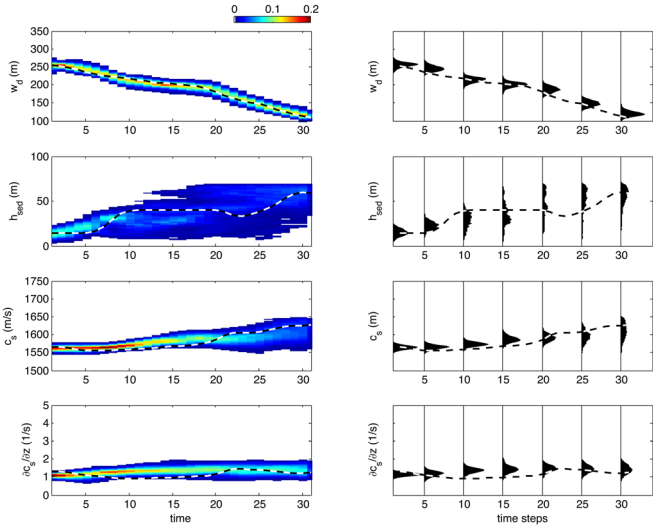

FIG. 9. (Color online) SWellEx-96 SIR-type PF results: Variation of 1-D marginal filtering posterior PDFs for sediment parameters. Lines represent the measured water depth and environmental parameters extracted from the Bachman profile (Refs. 20 and 53). The marginal PDFs with 5 time step increments also are plotted on the right.

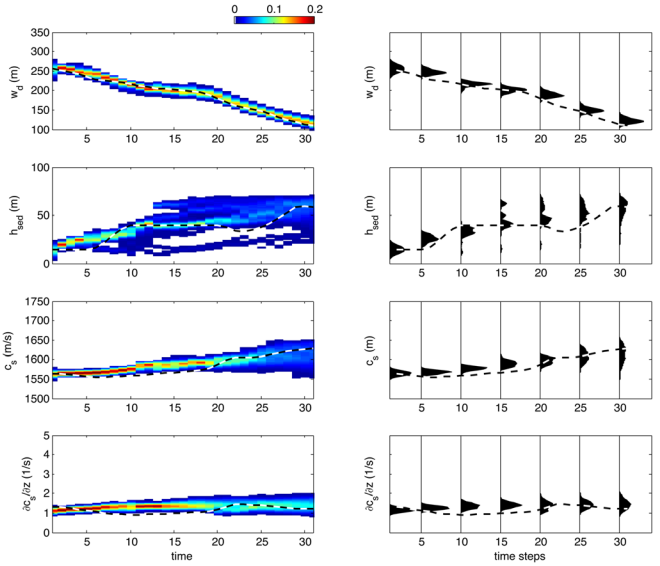

FIG. 10. (Color online) SWellEx-96 SIR-type FBS results: Variation of 1-D marginal smoothing posterior PDFs for sediment parameters. Lines represent the measured water depth and environmental parameters extracted from the Bachman profile (Refs. 20 and 53). The marginal PDFs with 5 time step increments also are plotted on the right.

each inversion/track step (13 CSDMs in total for each 1 min section). The CSDMs are computed with snapshots of 8192 point FFTs with 50% overlap between successive FFTs. The state consists of source depth, range, and speed, VLA tilt, water depth, sediment thickness, sediment top layer sound speed, and the slope of the sound speed in the sediment.

The environmental variation at the moving source location is shown in Ref. 20. Although the propagation is range-dependent, the environmental parameters change gradually between the source and the receiver. Thus, the adiabatic normal mode model SNAPRD[54] is used. This assumes all energy in a given mode at source location transfers to the corresponding mode at the VLA environment, neglecting cross-coupling terms.[55] The gradual range dependence is incorporated by calculating the mode functions at the source and receiver locations and linearly interpolating the wave numbers along the track. The environmental model given in Fig. 2 is adopted at the location of source and VLA. The environment at the fixed VLA location is assumed known and the environment at the moving source location is tracked.

B. Filtering and smoothing results

The results are given in Figs. 9 and 10 for the PF and FBS, respectively, and summarized in Table I. Ground truth at the location of the moving ship is given by fitting Bachman's results for the SWellEx-96 region[53] to the environmental model shown in Fig. 2 (see Appendix of Ref. 20).

TABLE II. SWellEx-96 Filter-smoother comparison.

Parameter	wd (m)	h_{sed} (m)	c_{sed} (m/s)	$\frac{\partial c_{sed}}{\partial z}$ (1/s)	Avg.
RTAMS_{PF}	12.1	16.8	21.7	0.3	-
$\text{RTAMS}_{\text{FBS}}$	9.3	15.6	18.3	0.2	-
FBS % improv.	23	7	16	10	14

The results show that, even thought the water depth changes from 260 to 100 m, the gradual slope enables the adiabatic normal mode based propagation model to compute the acoustic field adequately. There is an increased uncertainty in the parameters as water depth drops which may be due to secondary effects such as 3-D acoustic propagation and increasing errors in the adiabatic assumption.

All the parameters generally follow Bachman's ground truth results. Increases in both the sediment thickness and sediment sound speed are captured well. Both the PF and FBS are able to capture the rapidly decreasing water depth even though their state equations assumed a constant environment between the time steps. However, there is a larger amount of uncertainty compared to the previous example. A contributing factor is the increased state noise that allows the PF and smoother to continue tracking this rapidly evolving environment.

The PDFs of the PF given in Fig. 9 show a larger uncertainty compared to smoothing PDFs in Fig. 10. However, the average FBS improvement is 14% (Table II), lower than those of the previous example. The only parameter that has over 20% improvement is the water depth track. Note how running a PF forward and doing a backward correction affects the PDFs. For example, compare the marginal filtering posterior PDF cuts of h_{sed} at $t = 15$ to the FBS results where the PF results have a peak at the wrong value. Once a backward correction is run on the same PF results, the MAP solutions perfectly coincide with the ground truth.

VII. CONCLUSIONS

The concept of smoothing in sequential geoacoustic inversion has been discussed. The difference between a filter that uses previous data obtained up to and including the current time, and a smoother that uses data from the entire dataset (including future data) was explained.

Two main smoothing frameworks were compared, the forward-backward and the two-filter smoothers, including a modified two-filter smoother with reduced number of computations (the two-ASIR smoother). The filters and smoothers were used to process both SW06 and SWellEx-96 data. The results showed that both smoothing algorithms reduced uncertainties in both the environmental and source parameters. In general, the two-filter smoothers performed better than the forward-backward smoothers but the computational cost of the two-filter smoother also is higher.

The results showed that the uncertainty in the geoacoustic parameter estimates can be reduced using smoothers. It is important to keep in mind that there are numerous underlying acoustic and environmental assumptions in all geoacoustic inversion techniques such as simplified environmental models and their range dependencies, the assumptions used in the propagation models, and receiving array characterization (e.g., channel gains). None of these are incorporated into the inversion algorithms and will result in errors unaccounted for in the posterior PDFs.

ACKNOWLEDGMENT

This work was supported by the Office of Naval Research, under grant numbers N00014-11-1-0320.

APPENDIX: ASIR FILTER AND SMOOTHERS

The ASIR is a modified version of the standard SIR where the resampling stage is moved before the prediction stage for improved performance. Another difference in ASIR is that it uses a function μ_t^i that represents $\mathbf{x}_t$. Commonly used functions are $\mu_t^i = \mathrm{E}[\mathbf{x}_t|\mathbf{x}_{t-1}^i]$ or a sample from $\mu_t^i \sim p(\mathbf{x}_t|\mathbf{x}_{t-1}^i)$. Once a suitable μ_t^i is selected the ASIR performs resampling, prediction, and update at each t as shown in Table III.

TABLE III. ASIR PF (Ref. 33).

Resample

Calculate μ_t^i

Compute and normalize β_t^i $\beta_t^i = \dfrac{p(\mathbf{y}_t|\mu_t^i)w_{t-1}^i}{\sum_{i=1}^{N_p} p(\mathbf{y}_t|\mu_t^i)w_{t-1}^i}$

Resample new particles $\mathbf{x}_{t-1}^{j_i}$ with indices j_i from the old particles $\mathbf{x}_{t-1}^i$ using β_t^i $\{\mu_t^i, \beta_t^i\}_{i=1}^{N_p} \mapsto \{j_i\}_{i=1}^{N_p}$

Predict

Sample new N_p particles at t

$\{\mathbf{x}_t^i\}_{i=1}^{N_p} \sim p(\mathbf{x}_t|\mathbf{x}_{t-1}^{j_i})$ given $\{\mathbf{x}_{t-1}^{j_i}\}_{i=1}^{N_p}$ using $\{\mathbf{x}_t^i\} = \mathbf{f}_t(\mathbf{x}_{t-1}^{j_i}, \mathbf{v}_t^i)$ $i = 1, \ldots, N_p$ where $\mathbf{v}_t^i$ are samples from the state noise PDF.

Update

Compute the likelihood $p(\mathbf{y}_t|\mathbf{x}_t^i)$ for each $\mathbf{x}_t^i$

Normalize the weights: $w_t^i = \dfrac{p(\mathbf{y}_t|\mathbf{x}_t^i)\,/\,p(\mathbf{y}_t|\mu_t^{j_i})}{\sum_{i=1}^{N_p} p(\mathbf{y}_t|\mathbf{x}_t^i)\,/\,p(\mathbf{y}_t|\mu_t^{j_i})}$

The posterior PDF is approximated by $p(\mathbf{x}_t|\mathbf{y}_{1:t}) \approx \sum_{i=1}^{N_p} w_t^i \delta(\mathbf{x}_t - \mathbf{x}_t^i)$

The two-ASIR smoother given in Ref. 29 is a modified TFS that specifically enables sampling new particles representing the smoothing density. This smoother uses forward ASIR results $\{\mathbf{x}_{t-1}^i, w_{t-1}^i\}_{i=1}^{N_p}$ at $t-1$ and backward ASIR results at $\{\tilde{\mathbf{x}}_{t+1}^i, \tilde{w}_{t+1}^i\}_{i=1}^{N_p}$ at $t+1$ to sample a new set of smoothing particles $\{\bar{\mathbf{x}}_t^i\}_{i=1}^{N_p}$ that correspond to the underlying smoothing PDF as shown in Fig. 1(c).

Following the ASIR algorithm given above, Sec. III, and defining $\bar{(\cdot)}$ as the quantities related to smoothing, the two-ASIR smoother needs the following inputs:

(1) An ASIR weight $\bar{\beta}_t^{(j,k)} \cong \beta_t^{j_i}\tilde{\beta}_t^{k_i}$, obtained from the β_t values of the forward and backward ASIRs (see Table III);
(2) Some function $\bar{\mu}_t^i = f(\mathbf{x}_{t-1}^{j_i}, \tilde{\mathbf{x}}_{t+1}^{k_i})$ for the jth particle of the forward PF and kth particle of the backward PF;
(3) A suitable sampling density for the prediction stage $\bar{q}(\bar{\mu}_t^i|\mathbf{x}_{t-1}^{j_i}, \mathbf{y}_t, \tilde{\mathbf{x}}_{t+1}^{k_i})$.

The smoothing weight then can be computed as[29]

$$\bar{w}_t^i \propto \frac{p(\bar{\mathbf{x}}_t^i|\mathbf{x}_{t-1}^{j_i})p(\mathbf{y}_t|\bar{\mathbf{x}}_t^i)p(\tilde{\mathbf{x}}_{t+1}^{k_i}|\bar{\mathbf{x}}_t^i)w_{t-1}^{j_i}\tilde{w}_{t+1}^{k_i} \,/\, \tilde{p}(\tilde{\mathbf{x}}_{t+1}^{k_i})}{\bar{q}(\bar{\mathbf{x}}_t^i|\mathbf{x}_{t-1}^{j_i}, \mathbf{y}_t, \tilde{\mathbf{x}}_{t+1}^{k_i})\beta_t^{j_i}\tilde{\beta}_t^{k_i}}. \tag{A1}$$

The two-ASIR smoother is summarized in Table IV.

TABLE IV. Two-ASIR particle smoother (Ref. 29).

Forward ASIR

Compute and store $\{\mathbf{x}_t^i, w_t^i, \beta_t^i\}_{i=1}^{N_p}$ for $t = 1, \ldots, T$

$p(\mathbf{x}_t|\mathbf{y}_{1:t}) \approx \sum_{i=1}^{N_p} w_t^i \delta(\mathbf{x}_t - \mathbf{x}_t^i)$

Backward ASIR

Compute and store $\{\tilde{\mathbf{x}}_t^i, \tilde{w}_t^i, \tilde{\beta}_t^i\}_{i=1}^{N_p}$ for $t = T, \ldots, 1$

$\tilde{p}(\mathbf{x}_t|\mathbf{y}_{t:T}) \approx \sum_{i=1}^{N_p} \tilde{w}_t^i \delta(\mathbf{x}_t - \tilde{\mathbf{x}}_t^i)$

Resample

To sample a smoothing particle $\bar{\mathbf{x}}_t^i$ at time t

Resample new forward PF particles $\mathbf{x}_{t-1}^{j_i}$ with indices j_i from the old particles $\mathbf{x}_{t-1}^i$ using β_t^i $\{\mathbf{x}_{t-1}^i, \beta_t^i\}_{i=1}^{N_p} \mapsto \{j_i\}_{i=1}^{N_p}$

Resample new backward particles $\tilde{\mathrm{x}}_{t-1}^{k_i}$ with indices k_i from the old particles $\tilde{\mathbf{x}}_{t+1}^i$ using $\tilde{\beta}_t^i$ $\{\tilde{\mathbf{x}}_{t+1}^i, \tilde{\beta}_t^i\}_{i=1}^{N_p} \mapsto \{k_i\}_{i=1}^{N_p}$

Predict

Using the forward particle at $t-1$, backward particle at $t+1$, and the current measurement $\mathbf{y}_t$ obtain smoothing particle

$\{\bar{\mathbf{x}}_t^i\}_{i=1}^{N_p} \sim \bar{q}(\bar{\mathbf{x}}_t^i|\mathbf{x}_{t-1}^{j_i}, \mathbf{y}_t, \tilde{\mathbf{x}}_{t+1}^{k_i})$

Update

Compute $\bar{w}_t^i$ from Eq. (A1) $\rightarrow$ normalize $\bar{w}_t^i = \dfrac{\bar{w}_t^i}{\sum_{i=1}^{N_p} \bar{w}_t^i}$

$p(\mathbf{x}_t|\mathbf{y}_{1:T}) \approx \sum_{i=1}^{N_p} \bar{w}_t^i \delta(\mathbf{x}_t - \bar{\mathbf{x}}_t^i)$

[1]B. Ristic, S. Arulampalam, and N. Gordon, *Beyond the Kalman Filter: Particle Filters for Tracking Applications* (Artech House, Boston, MA, 2004), Chaps. 1–3.
[2]O. Cappé, S. Godsill, and E. Moulines, "An overview of existing methods and recent advances in sequential Monte Carlo," Proc. IEEE **95**, 899–924 (2007).
[3]J. V. Candy, *Bayesian Signal Processing: Classical, Modern and Particle Filtering Methods* (John Wiley and Sons, Hoboken, NJ, 2009), Chap. 7.
[4]S. E. Dosso and M. J. Wilmut, "Uncertainty estimation in simultaneous Bayesian tracking and environmental inversion," J. Acoust. Soc. Am. **124**, 82–97 (2008).
[5]M. Briers, A. Doucet, and S. R. Maskell, "Smoothing algorithms for state-space models," Ann. Inst. Stat. Math. **62**, 61–89 (2010).
[6]P. Gerstoft, "Inversion of seismoacoustic data using genetic algorithms and *a posteriori* probability distributions," J. Acoust. Soc. Am. **95**, 770–782 (1994).
[7]A. Tolstoy, N. R. Chapman, and G. Brooke, "Workshop 97: Benchmarking for geoacoustic inversion in shallow water," J. Comput. Acoust. **6**, 1–28 (1998).
[8]J. Hermand, "Broad-band geoacoustic inversion in shallow water from waveguide impulse response measurements on a single hydrophone: Theory and experimental results," IEEE J. Ocean. Eng. **24**, 41–66 (1999).
[9]S. E. Dosso, "Quantifying uncertainty in geoacoustic inversion I. A fast Gibbs sampler approach," J. Acoust. Soc. Am. **111**, 129–142 (2002).
[10]N. R. Chapman, S. Chin-Bing, D. King, and R. B. Evans, "Benchmarking geoacoustic inversion methods for range-dependent waveguides," IEEE J. Ocean. Eng. **28**, 320–330 (2003).
[11]M. R. Fallat, P. L. Nielsen, S. E. Dosso, and M. Siderius, "Geoacoustic characterization of a range-dependent ocean environment using towed array data," IEEE J. Ocean. Eng. **30**, 198–206 (2005).
[12]G. R. Potty, J. H. Miller, P. S. Wilson, J. F. Lynch, and A. Newhall, "Geoacoustic inversion using combustive sound source signals," J. Acoust. Soc. Am. **124**, EL146–EL150 (2008).
[13]M. S. Ballard and K. M. Becker, "Geoacoustic inversion on the New Jersey Margin: Along and across the shelf," J. Acoust. Soc. Am. **124**, EL141–EL145 (2008).
[14]D. P. Knobles, P. S. Wilson, J. A. Goff, and S. E. Cho, "Seabed acoustics of a sand ridge on the New Jersey continental shelf," J. Acoust. Soc. Am. **124**, EL151–EL156 (2008).
[15]J. V. Candy and D. H. Chambers, "Model-based dispersive wave processing: A recursive Bayesian solution," J. Acoust. Soc. Am. **105**, 3364–3374 (1999).
[16]E. J. Sullivan, J. D. Holmes, W. M. Carey, and J. F. Lynch, "Broadband passive synthetic aperture: Experimental results," J. Acoust. Soc. Am. **120**, EL49–EL54 (2006).
[17]C. He, J. E. Quijano, and L. M. Zurk, "Enhanced Kalman filter algorithm using the invariance principle," IEEE J. Ocean. Eng. **34**, 575–585 (2009).
[18]O. Carrière, J.-P. Hermand, J.-C. Le Gac, and M. Rixen, "Full-field tomography and Kalman tracking of the range-dependent sound speed field in a coastal water environment," J. Mar. Syst. **78**, S382–S392 (2009).
[19]C. Yardim, P. Gerstoft, and W. S. Hodgkiss, "Tracking of geoacoustic parameters using Kalman and particle filters," J. Acoust. Soc. Am. **125**, 746–760 (2009).
[20]C. Yardim, P. Gerstoft, and W. S. Hodgkiss, "Geoacoustic and source tracking using particle filtering: Experimental results," J. Acoust. Soc. Am. **128**, 75–87 (2010).
[21]J. Dettmer, S. E. Dosso, and C. W. Holland, "Sequential trans-dimensional Monte Carlo for range-dependent geoacoustic inversion," J. Acoust. Soc. Am. **129**, 1794–1806 (2011).
[22]C. Yardim, P. Gerstoft, and W. S. Hodgkiss, "Sequential geoacoustic inversion at the continental shelfbreak," J. Acoust. Soc. Am. **131**, 1722–1732 (2012).
[23]Z.-H. Michalopoulou, C. Yardim, and P. Gerstoft, "Particle filtering for passive fathometer tracking," J. Acoust. Soc. Am. **131**, EL74–EL80 (2012).
[24]O. Carrière and J. Hermand, "Sequential Bayesian geoacoustic inversion for mobile and compact source-receiver configuration," J. Acoust. Soc. Am. **131**, 2668–2681 (2012).
[25]I. Zorych and Z.-H. Michalopoulou, "Particle filtering for dispersion curve tracking in ocean acoustics," J. Acoust. Soc. Am. **124**, EL45–EL50 (2008).
[26]R. Jain and Z.-H. Michalopoulou, "A particle filtering approach for spatial arrival time tracking in ocean acoustics," J. Acoust. Soc. Am. **129**, EL236–EL241 (2011).
[27]G. Kitagawa, "Monte Carlo filter and smoother for non-Gaussian nonlinear state space models," J. Comput. Graphical Stat. **5**, 1–25 (1996).
[28]M. Klaas, M. Briers, N. De Freitas, A. Doucet, S. Maskell, and D. Lang, "Fast particle smoothing: If I had a million particles," in *Proc. International Conference on Machine Learning*, 481–488 (ACM) (2006).
[29]P. Fearnhead, D. Wyncoll, and J. Tawn, "A sequential smoothing algorithm with linear computational cost," Biometrika **97**, 447–464 (2010).
[30]M. Arulampalam, S. Maskell, N. Gordon, and T. Clapp, "A tutorial on particle filters for online nonlinear/non-Gaussian Bayesian tracking," IEEE Trans. Signal Processing **50**, 174–188 (2002).
[31]L. Rabiner and B. Juang, "An introduction to hidden Markov models," IEEE ASSP Mag. **3**, 4–16 (1986).
[32]N. J. Gordon, D. J. Salmond, and A. F. M. Smith, "Novel approach to nonlinear/non-Gaussian Bayesian state estimation," IEE Proc. F **140**, 107–113 (1993).
[33]M. K. Pitt and N. Shephard, "Filtering via simulation: Auxiliary particle filters," J. Am. Stat. Assoc. **94**, 590–599 (1999).
[34]C. Yardim, Z.-H. Michalopoulou, and P. Gerstoft, "An overview of sequential Bayesian filtering in ocean acoustics," IEEE J. Ocean. Eng. **36**, 71–89 (2011).
[35]A. Doucet, S. Godsill, and C. Andrieu, "On sequential Monte Carlo sampling methods for Bayesian filtering," Stat. Comput. **10**, 197–208 (2000).
[36]C. Yardim and P. Gerstoft, "Sequential Bayesian techniques applied to non-volcanic tremor," J. Geophys. Res. **117**, B10312, doi:10.1029/2012JB009420 (2012).
[37]C.-F. Huang, P. Gerstoft, and W. S. Hodgkiss, "Effect of ocean sound speed uncertainty on matched-field geoacoustic inversion," J. Acoust. Soc. Am. **123**, EL162–EL168 (2008).
[38]Y. M. Jiang and N. R. Chapman, "Bayesian geoacoustic inversion in a dynamic shallow water environment," J. Acoust. Soc. Am. **123**, EL155–EL161 (2008).
[39]F. B. Jensen and M. C. Ferla, *SNAP: The SACLANTCEN normal-mode acoustic propagation model*, SM-121 (SACLANT Undersea Research Center, La Spezia, Italy, 1979), pp. 1–109.
[40]J. Choi, P. Dahl, and J. Goff, "Observations of the R reflector and sediment interface reflection at the Shallow Water'06 Central Site," J. Acoust. Soc. Am. **124**, El128–EL134 (2008).
[41]Y. M. Jiang, N. R. Chapman, and P. Gerstoft, "Short range travel time geoacoustic inversion with a vertical line array," J. Acoust. Soc. Am. **124**, EL135–EL140 (2008).
[42]M. S. Ballard, K. M. Becker, and J. A. Goff, "Geoacoustic inversion for the New Jersey shelf: 3-D sediment model," IEEE J. Ocean. Eng. **35**, 28–42 (2010).
[43]D. P. Knobles, J. A. Goff, R. A. Koch, P. S. Wilson, and J. A. Shooter, "Effect of inhomogeneous sub-bottom layering on broadband acoustic propagation," IEEE J. Ocean. Eng. **35**, 732–743 (2010).
[44]J. Yang, D. Tang, and K. L. Williams, "Direct measurement of sediment sound speed in Shallow Water'06," J. Acoust. Soc. Am. **124**, EL116–EL121 (2008).
[45]T. Bengtsson, P. Bickel, and B. Li, "Curse-of-dimensionality revisited: Collapse of the particle filter in very large scale systems," IMS Coll. **2**, 316–334 (2008).
[46]F. Daum and J. Huang, "Curse of dimensionality and particle filters," in. *Proceedings of the 2003 IEEE Aerospace Conference* (Big Sky, MT), Vol. 4, pp. 1979–1993.
[47]P. Del Moral, *Feynman-Kac Formulae: Genealogical and Interacting Particle Systems With Applications* (Springer Verlag, New York, 2004), pp. 1–575.
[48]Y.-H. Goh, P. Gerstoft, W. S. Hodgkiss, and C.-F. Huang, "Statistical estimation of transmission loss from geoacoustic inversion using a towed array," J. Acoust. Soc. Am. **122**, 2571–2579 (2007).
[49]C.-F. Huang, P. Gerstoft, and W. S. Hodgkiss, "Validation of statistical estimation of transmission loss in the presence of geoacoustic inversion uncertainty," J. Acoust. Soc. Am. **120**, 1932–1941 (2006).
[50]J. J. K. Ó Ruanaidh and W. J. Fitzgerald, *Numerical Bayesian Methods Applied to Signal Processing* (Springer-Verlag, New York, 1996), pp. 51–54.
[51]A. Doucet and A. M. Johansen, "A tutorial on particle filtering and smoothing: Fifteen years later," in *The Oxford Handbook of Nonlinear Filtering* (Oxford University Press, New York, 2009), Chap. 8.
[52]N. O. Booth, A. T. Abawi, P. W. Schey, and W. S. Hodgkiss, "Detectability of low-level broad-band signals using adaptive matched-field processing with vertical aperture arrays," IEEE J. Ocean. Eng. **25**, 296–313 (2000).
[53]R. T. Bachman, P. W. Schey, N. O. Booth, and F. J. Ryan, "Geoacoustic databases for matched-field processing: Preliminary results in shallow water off San Diego, California," J. Acoust. Soc. Am. **99**, 2077–2085 (1996).
[54]P. Gerstoft, *SAGA Users guide 5.4, An Inversion Software Package*, An updated version of "SAGA 2.0", SM-333 (SACLANT Undersea Research Centre, La Spezia, Italy, 1997), pp. 1–115.
[55]F. B. Jensen, W. A. Kuperman, M. B. Porter, and H. Schmidt, *Computational Ocean Acoustics* (Springer-Verlag, New York, 2000), pp. 304–307.